 DOI 10.1109/JETCAS.2015.2462017

Nonlinear Analysis of Interconnected Power Converters: a case study

Luis Benadero, Rony Cristiano, Daniel J. Pagano, *Member, IEEE*, and Enrique Ponce

***Abstract*—In this paper the nonlinear dynamics of interconnected power converters in an islanded direct current (DC) microgrid is analyzed. By using a simplified scheme based on two cascaded converters we analyze the dynamical behavior that can arise from the interconnection of these devices on a common DC bus. Furthermore, in order to address the bus voltage control problem, we propose a Sliding Mode Controller for a DC-DC bidirectional power converter to control the DC bus voltage under instantaneous Constant Power Loads (CPLs). This class of loads introduces a destabilizing nonlinear effect on the converter through an inverse voltage term that can lead to significant oscillations in the DC bus voltage. Simulation results are shown to illustrate the nonlinear analysis.**

***Index Terms*—DC microgrids, Boost converter, Constant power load, Sliding mode control, Nonlinear analysis, Bifurcations**

I. INTRODUCTION

THE increasing energy demand associated with environmental concerns has driven the electric power systems to the distributed generation using renewable energy sources. This is due to the high cost of large centralized generation plants that have low efficiency and poor reliability, in addition to requiring, mostly fuel fossil [1]. Despite the discussions regarding the advantages and disadvantages of DC and *alternating current* (AC) distribution systems (see [2]), it is common sense that for facing the energy sector challenges in an economically efficient way, the first step is to maximize the use of resources by improving the ways of consuming electricity. As a way to overcome AC distribution problems, DC microgrids are discussed and analyzed as a solution for new ways of power distribution.

In modern electrical distribution systems, switched power converters are used to connect the different elements given by distribution generation systems, storage elements and loads to the main DC microgrid. Nowadays, one of the most widely studied topologies of power converters interconnection is the cascade structure. In [3], a systematic procedure to synthesize cascade connection of DC-DC boost converters operating with sliding mode control is presented. This method is applied to a system connected to a photovoltaic source consisting of two cascaded DC-DC boost converters under sliding mode control in [4]. Smooth and non-smooth bifurcations in multi-structure multi-operating-mode hybrid power systems are studied in [5] where a hybrid power system consisting of dual-input buck converters is analysed. Moreover, a stand-alone photovoltaic-battery hybrid power system is analysed using standard bifurcation analysis based on averaged models in [6]. In [7], a comparative study of several nonlinear control techniques (Immersion and Invariance, Passivity-Based Control, Feedback Linearization and Sliding-Mode Control) applied to dc-dc power converters was presented.

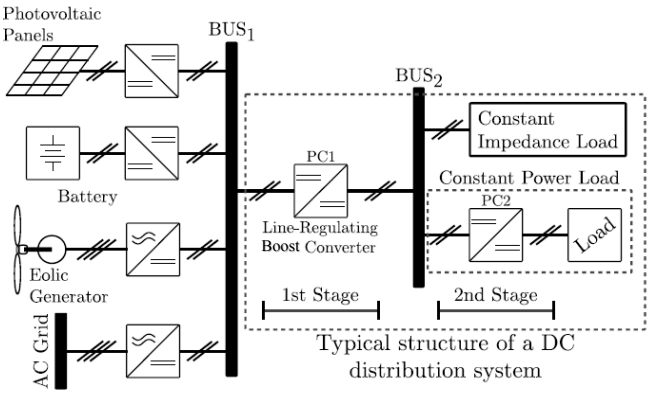

Figure 1. DC microgrid system.

This work presents the nonlinear dynamical analysis of a structure generally exhibited in DC microgrids [8], a cascade of two boost converters, as depicted in Fig. 1. A bidirectional power converter (PC1) is connected to the main bus (BUS1) where several sources and loads are connected. This converter is responsible for regulating the voltage of the bus, which is subject to unknown loads and to the fluctuation of parallel sources. We are interested in this paper, in analyzing the control problems imposed by the connection of tightly regulated point-of-load converters [9].

A simplified schematic diagram corresponding to our case study is depicted in Fig. 2, showing two boost converters connected to a common BUS2 together with a resistive load. Since the input and output power of PC2 (P_{in} and P_o) are constant in steady-state, the static input v-i characteristic is ideally a hyperbola defined for $v > 0$ and $i > 0$. For that reason, PC2 can be modeled as a *constant power load* (CPL). Consequently, the second converter (PC2) as seen by PC1, has a negative impedance characteristics, where a voltage increment will cause a current decrease and vice versa.

The PC1 converter in Fig 1 can be analyzed by the simpli-

Daniel J. Pagano and R. Cristiano are with the Dept. of Automation and Systems, Federal University of Santa Catarina, Florianópolis, Brazil (e-mail: daniel.pagano@ufsc.br, rony.cristiano@ufsc.br).

Enrique Ponce is with the Dept. of Applied Mathematics, University of Seville, Seville, Spain (e-mail: eponcem@us.es).

L. Benadero is with the Dept. of Applied Physics, Technical University of Catalonia, Barcelona, Spain (email: luis@fa.upc.edu).

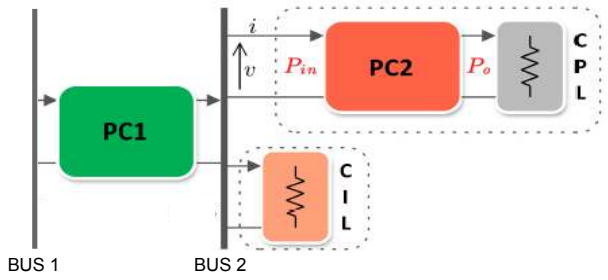

Figure 2. Two interconnected power converters on a common DC bus with a resistive load (CIL).

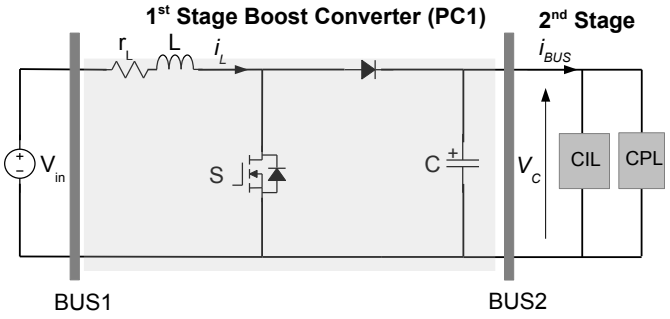

Figure 3. Structure of the first stage boost converter.

fied model depicted in Fig 3, composed by the main boost converter that feeds a CPL and a *constant impedance load* (CIL). A CIL represents any kind of load where the impedance does not change with variations of voltage or current magnitude. In this study, the nonlinear analysis of the BUS2 is made, by considering that the equivalent load seen from PC1 is highly nonlinear and has a piecewise defined characteristic dependent on the point of load operation (see Fig. 4), assuming both CPL and CIL characteristics. Comparing to the classical CPL modeling [10], this load characteristic leads to a more realistic representation of the actual system operation.

Here, the proposed controller uses a *sliding mode control* (SMC) technique based on the nonlinear model of the system and an adaptive scheme to reject unknown load variations. The study also presents a stability analysis for the nonlinear model of the cascaded converters, putting emphasis on the importance of bifurcation analysis for the sliding dynamics.

Thus, the interconnected system studied in this work will deal with a realistic load profile, where the CPL is represented by a second stage boost converter with an independent control loop. For PC2 being able to regulate its output voltage to a predefined reference, the bus voltage needs to be greater than a threshold voltage (V_{th}), therefore, determining the equivalent system two regions of different behavior. Some preliminary results following the same approach for a different case were presented in [11].

The paper is organized as follows. The modeling of the boost power converter and of the constant power load (CPL) are developed in Section II. Nonlinear analysis of the interconnected power converters case is presented in Section III. Simulation results to illustrate the developed nonlinear analysis are shown in Section IV. Some conclusions are offered in the last section. Moreover, a short review of the relevant concepts in the analysis of discontinuous control systems through dynamical systems theory and bifurcation theory, fixing also the notation to be followed in the paper, is also given in Appendix.

II. MODELING OF THE INTERCONNECTED CONVERTERS

A. Boost converter $PC1$

The behavior of a boost converter can be studied using the circuit topology depicted in Fig. 3. Using the Kirchhoff's circuit laws, the dynamic model of the system is given by

$$\begin{cases} C\dfrac{dv_c(t)}{dt} &= ui_L(t) - i_{\mathrm{BUS2}}(t), \\ L\dfrac{di_L(t)}{dt} &= V_{in} - uv_c(t) - r_L i_L(t) \end{cases} \tag{1}$$

where $v_c(t)$ and $i_L(t)$ are the instantaneous capacitor's voltage and the inductor's current, respectively. The BUS1 input voltage is assigned as V_{in}, r_L is the equivalent series resistance of the inductor, C and L are the circuit's capacitor and inductor respectively and i_{BUS2} is the current flowing through the loads attached to the bus, defined as $i_{\mathrm{BUS2}} = \frac{v_c}{R} + \Phi(v_c)$, where

$$\Phi(v_c) = \begin{cases} i_{max}, & \text{for } v_c < v_{th} \\ \dfrac{P}{v_c}, & \text{for } v_c \geq v_{th} \end{cases}, \tag{2}$$

R is a resistive load, P is the constant power load and i_{max} is the maximum value fixed for the current in PC2. The switching function u assumes binary values $u \in \{0, 1\}$, thus representing the states of the switch S closed (on) for $u = 0$ and opened (off) for $u = 1$ respectively.

To ease visualization and analysis of the model, the system is normalized using the following change of variables

$$v_c(t) = V_{in}x_1(\tau) \quad i_L(t) = \sqrt{\frac{C}{L}}V_{in}x_2(\tau) \tag{3}$$

and time $t = \tau\sqrt{LC}$. Defining the new parameters

$$b = r_L\sqrt{\frac{C}{L}} \qquad \gamma_R = \frac{1}{R}\sqrt{\frac{L}{C}} \qquad \gamma_P = \frac{P}{V_{in}^2}\sqrt{\frac{L}{C}}, \tag{4}$$

the dimensionless model is given by

$$\begin{cases} \dot{x}_1(\tau) &= -\gamma_R x_1(\tau) - \xi(x_1) + ux_2(\tau) \\ \dot{x}_2(\tau) &= -ux_1(\tau) - bx_2(\tau) + 1 \end{cases}, \tag{5}$$

where

$$\xi(x_1) = \begin{cases} x_2^*, & \text{for } x_1 < x_{th} \\ \dfrac{\gamma_P}{x_1}, & \text{for } x_1 \geq x_{th} \end{cases} \tag{6}$$

where $x_2^* = i_{max}\sqrt{L/C}/V_{in}$ is the maximum value fixed for the normalized current in PC2 and x_{th} is the normalized

threshold voltage. Parameters γ_R and γ_P stand for the normalized resistive and power loads of the circuit system, respectively. These parameters vary with the power demand and the availability of sources on the microgrid, thus causing changes in the system dynamics and uncertainty on the location of the desired operating point (pseudo-equilibrium) in the state space.

B. Constant Power Load (PC2)

As previously stated, microgrid power converters usually deal with two main kinds of loads: constant impedance loads (CIL) and second stage converters behaving ideally as constant power loads (CPL). An idealistic boost converter with no parasitic losses, operating with minimum duty cycle, provides an output equal to its input voltage. When operating with maximum duty cycle, it can provide, theoretically, an infinite output voltage. However, when the losses are considered, the ranges of output voltage and inductor's current are limited by the converter's load and by the losses itself.

The boost converter acting here as the second stage load converter (PC2) has the same structure of PC1. It has its own controller, designed to operate in a predefined voltage reference and also to limit the maximum inductor's current according to the circuit's limitations. From the interconnected model in Fig. 3, the BUS2 current (x_2^{BUS2}) is given by

$$x_2^{\mathrm{BUS2}} = x_2^{\mathrm{CIL}} + x_2^{\mathrm{PC2}} = \gamma_R x_1 + \xi(x_1), \tag{7}$$

where $\xi(x_1)$ is a piecewise defined function (6) that describes the second stage converter (PC2) load profile.

Since PC2's maximum current is limited by its own controller, when the input voltage is below a certain threshold, the current is saturated at the maximum value while the output voltage can not reach its reference. The threshold from which PC2 starts operating can be calculated using the equation

$$x_{th} = \frac{\gamma_P}{x_2^*}, \tag{8}$$

so that in $x_1 = x_{th}$ the function is continuous (but not differentiable), as shown in Figure 4.

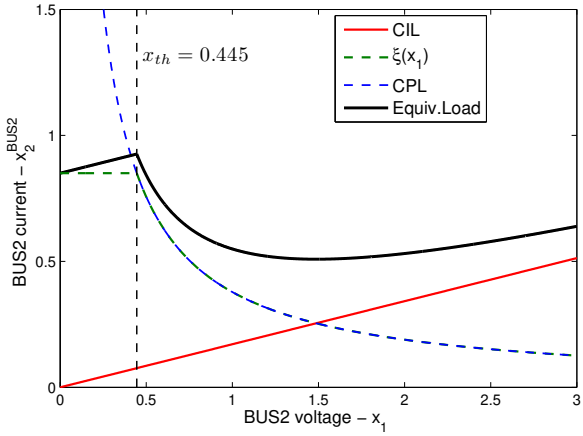

Figure 4. Equivalent load for the system in Fig. 3, showing the voltage threshold x_{th} and the piecewise profiles.

Figures 5 and 6 shows the curves obtained for variations of γ_R and γ_P respectively. For a constant CPL, an increase

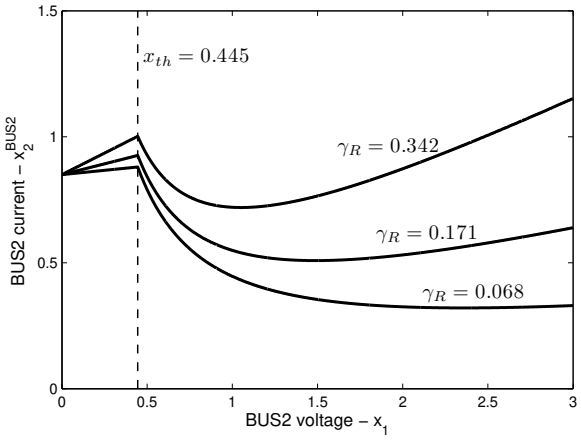

Figure 5. Equivalent load curves for the system in Fig. 3 for a fixed γ_P and different values of γ_R.

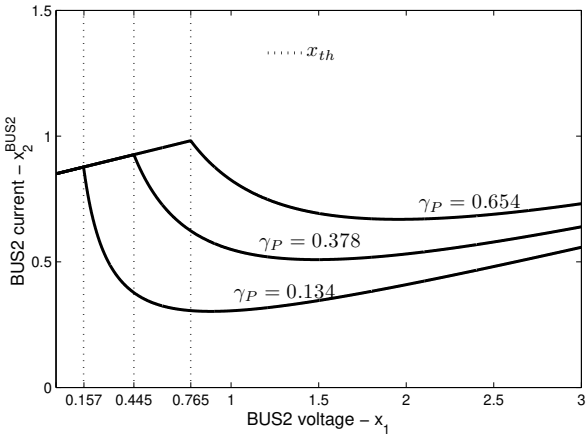

Figure 6. Equivalent load curves for the system in Fig. 3 for a fixed γ_R and different values of γ_P.

in the CIL power (reduction of R) shifts up the curve and changes its slope, but does not change the voltage threshold x_{th}. For a constant CIL (parameter γ_R), an increase in the CPL power (parameter γ_P) shifts up the curve and increases the voltage threshold x_{th}. These load changes have great effect when designing the control law.

From here on, time dependence on variables might be suppressed for the sake of clarity.

C. Washout-SMC

The power converter feeding the bus has no information on the load connected to it. Since its dynamics is dependent on these load variations, the equilibrium points of the controlled system are uncertain. Usually, dc-dc converters are controlled using linear techniques, which normally take a linearized model of the system. These techniques can guarantee zero state-error and have the advantage of having fixed switching

frequencies, but under unknown load variations their performance is degraded. In order to ensure robustness under load and source variations and minimizing transient responses, a *Sliding Mode Controller* (SMC) based on a washout filter is proposed.

A washout filter is a high pass filter that washes out steady state inputs, while passing transient inputs [12]. The main advantage of such method is the property of automatic equilibrium following, ensuring adaptation of the sliding surface under load variations [13]. The Washout-SMC was used because its better time-domain performance when compared to a conventional PWM-PI controller.

The inductor current x_2 is passed through a washout filter (see Fig. 7) and a new signal x_3 is obtained by the dynamic equation

$$\dot{x}_3 = \omega_n(x_2 - x_3), \tag{9}$$

where $\omega_n = \omega\sqrt{LC}$ is the normalized cut-off frequency of the filter, ω denotes the reciprocal of the filter constant in the physical system and $x_F = x_2 - x_3$ is the filtered normalized current.

The planar switching manifold is defined as

$$\Sigma = \{\mathbf{x} \in \mathbb{R}^3 : h(\mathbf{x}) = 0\},$$

where $\mathbf{x} = (x_1, x_2, x_3)$ and the switching surface is chosen as

$$h(\mathbf{x}) = x_1 - x_r + k(x_2 - x_3), \tag{10}$$

where $k > 0$ is the normalized control parameter to be adequately tuned and $x_r = \frac{v_r}{V_{in}} > 1$ is the normalized reference voltage. The physical control parameter is given by $K = k\sqrt{L/C}[\Omega]$. The control law is defined as

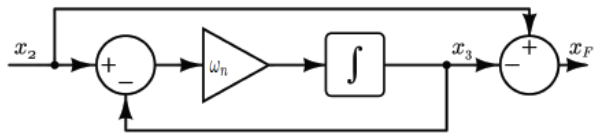

Figure 7. Washout filter block diagram.

$$u = \begin{cases} u^- = 0, & \text{if } h(\mathbf{x}) < 0 \\ u^+ = 1, & \text{if } h(\mathbf{x}) > 0. \end{cases} \tag{11}$$

D. System modeling

Assuming system (5) is operating in *continuous conduction mode* (CCM) and controlled by the SMC law given in (11), we conclude that for each switch state there is a different vector field representing the dynamics of the system. When the combined trajectories of the vector fields hit the switching surface ($h(\mathbf{x}) = 0$) inside the attractive region, the phenomena of sliding occurs. The chosen notation uses $\mathbf{f}^-(\mathbf{x})$ and $\mathbf{f}^+(\mathbf{x})$ to represent the vector fields for the switch $u = 0$ (case on) and $u = 1$ (case off), respectively. The dynamics of the system using the proposed SMC control with washout filter can be represented by the dynamical system

$$\dot{\mathbf{x}} = \begin{cases} \mathbf{f}^-(\mathbf{x}), & \text{if } h(\mathbf{x}) < 0 \\ \mathbf{f}^+(\mathbf{x}), & \text{if } h(\mathbf{x}) > 0, \end{cases} \tag{12}$$

composed by the vector fields

$$\mathbf{f}^-(\mathbf{x}) = \begin{bmatrix} -\gamma_R x_1 - x_2^* \\ -bx_2 + 1 \\ \omega_n(x_2 - x_3) \end{bmatrix}, \ \mathbf{f}^+(\mathbf{x}) = \begin{bmatrix} -\gamma_R x_1 + x_2 - x_2^* \\ -x_1 - bx_2 + 1 \\ \omega_n(x_2 - x_3) \end{bmatrix}$$

defined for $x_1 < x_{th}$, or

$$\mathbf{f}^-(\mathbf{x}) = \begin{bmatrix} -\gamma_R x_1 - \frac{\gamma_P}{x_1} \\ -bx_2 + 1 \\ \omega_n(x_2 - x_3) \end{bmatrix}, \ \mathbf{f}^+(\mathbf{x}) = \begin{bmatrix} -\gamma_R x_1 - \frac{\gamma_P}{x_1} + x_2 \\ -x_1 - bx_2 + 1 \\ \omega_n(x_2 - x_3) \end{bmatrix}$$

defined for $x_1 \geq x_{th}$.

III. Nonlinear Analysis

In this Section, we use the results given in Appendix A to analyze system (12). We begin the analysis considering separately the equilibria of the two vector fields involved by assuming the constraint $x_2 > 0$.

The vector field $\mathbf{f}^+$ can have up to three equilibria, one in the region $x_1 < x_{th}$ and two in $x_1 \geq x_{th}$ region. However, these equilibria are virtual. This is easy to be checked, because if $\mathbf{e}^+ = (\bar{x}_1, \bar{x}_2, \bar{x}_2)$ is the equilibrium in the region $x_1 < x_{th}$ then $h(\mathbf{e}^+) = \bar{x}_1 - x_r < 0$ since $\bar{x}_1 < x_{th} < x_r$. Now, if $\mathbf{e}^+_{2,3} = (\bar{x}_1^{(2,3)}, \bar{x}_2^{(2,3)}, \bar{x}_2^{(2,3)})$ are the equilibria in the region $x_1 \geq x_{th}$, then we also have $h(\mathbf{e}^+_{2,3}) = \bar{x}_1^{(2,3)} - x_r < 0$ because, of the equation

$$-(1 + \gamma_R b)x_1^2 + x_1 - b\gamma_P = 0,$$

from where one obtains the position at x_1 of these equilibria as a function of parameters (γ_P, γ_R, b), resulting in

$$\bar{x}_1^{(2)} \leq \bar{x}_1^{(3)} \leq \frac{1}{1 + \gamma_R b} < 1 < x_r.$$

The vector field $\mathbf{f}^-$ has no equilibria in its workspace, $x_1 > 0$ and $\gamma_P > 0$.

The sliding vector field is calculated from the equation (A.36), resulting in

$$\mathbf{f}_s(\mathbf{x}) = \begin{cases} \mathbf{f}_{s_1}(\mathbf{x}), & \text{if } x_1 < x_{th} \\ \mathbf{f}_{s_2}(\mathbf{x}), & \text{if } x_1 \geq x_{th}, \end{cases} \tag{13}$$

composed by the vector fields

$$\mathbf{f}_{s_1} = \begin{bmatrix} \frac{-k(\gamma_R x_1^2 + x_2^* x_1 - x_2 + bx_2^2) - k\omega_n x_2(x_2 - x_3)}{kx_1 - x_2} \\ \frac{\gamma_R x_1^2 + x_2^* x_1 - x_2 + bx_2^2 + k\omega_n x_1(x_2 - x_3)}{kx_1 - x_2} \\ \omega_n(x_2 - x_3) \end{bmatrix} \tag{14}$$

and

$$\mathbf{f}_{s_2} = \begin{bmatrix} \frac{-k(\gamma_R x_1^2 + bx_2^2 - x_2 + \gamma_P) - k\omega_n x_2(x_2 - x_3)}{kx_1 - x_2} \\ \frac{\gamma_R x_1^2 + bx_2^2 - x_2 + \gamma_P + k\omega_n x_1(x_2 - x_3)}{kx_1 - x_2} \\ \omega_n(x_2 - x_3) \end{bmatrix}. \tag{15}$$

The pseudo-equilibria points of system (12) are solutions of the equation system $\mathbf{f}_s(\mathbf{x}) = \mathbf{0}$ and $h(\mathbf{x}) = 0$, with scalar function h given in (10) and sliding vector field $\mathbf{f}_s$ in (14)-(15). Thus, these pseudo-equilibria have normalized voltage equal to the normalized reference voltage, that is, $\tilde{x}_1 = x_r$. Therefore, the system (13) has no pseudo-equilibria in the region $x_1 <$

x_{th}, because $x_r > x_{th}$. Thus, there are only pseudo-equilibria in the region $x_1 \geq x_{th}$, given by $\mathbf{p}^{\pm} = (x_r, \tilde{x}_2^{\pm}, \tilde{x}_2^{\pm})$, with

$$\tilde{x}_2^{\pm} = \frac{1 \pm \sqrt{1 - 4b(\gamma_P + \gamma_R x_r^2)}}{2b}. \tag{16}$$

Note that the points $\mathbf{p}^{\pm}$ only exist for

$$\gamma_P \leq \frac{1 - 4b\gamma_R x_r^2}{4b}. \tag{17}$$

For the stability study of pseudo-equilibria let us consider the vector fields defined for $x_1 > x_{th}$. Firstly, is important to know the position of these points on the switching boundary Σ, determining conditions on parameters so that $\mathbf{p}^{\pm}$ belong to the attractive region Σ_{as}. The analysis is easier if we project both Σ and $\mathbf{f}_s$ on the (x_1, x_2)-plane, reducing so the dimension of the problem by simply substituting $x_3 = x_3^{\Sigma} = \frac{x_1 - x_r + kx_2}{k}$. Thus, the projection of Σ_{as} is given by (A.33)

$$(\omega_n - \gamma_R)x_1 - bkx_2 - \frac{\gamma_P}{x_1} + k - \omega_n x_r > 0 \tag{18}$$

$$(\omega_n - \gamma_R - k)x_1 + (1 - bk)x_2 - \frac{\gamma_P}{x_1} + k - \omega_n x_r < 0 \tag{19}$$

where we already have done the above substitution. From (18)-(19), all the points belonging to Σ fulfill the condition $kx_1 - x_2 > 0$, and so we can desingularize the sliding vector field by considering the vector field $\mathbf{f}_{ds}(\mathbf{x}) = (kx_1 - x_2)\mathbf{f}_s(\mathbf{x})$. Moreover, the dynamics on the sliding mode can be analyzed in the (x_1, x_2)-plane, substituting again $x_3 = x_3^{\Sigma}$ and considering only the two first components of the desingularized sliding vector field $\mathbf{f}_{ds}$. Therefore, the differential equations that describe the dynamics on the sliding mode, projected on the (x_1, x_2)-plane, can be expressed as

$$\dot{x}_1 = -k(bx_2^2 - x_2 + \gamma_R x_1^2 + \gamma_P) + \omega_n x_2(x_1 - x_r), \tag{20}$$

$$\dot{x}_2 = bx_2^2 - x_2 + \gamma_R x_1^2 + \gamma_P - \omega_n x_1(x_1 - x_r) \tag{21}$$

for $kx_1 - x_2 > 0$, $x_1 > x_{th}$ and $x_2 > 0$.

The relevant equilibrium points for this reduced dynamical system are those with $x_1 = x_r$, namely, the solutions of the quadratic equation

$$bx_2^2 - x_2 + \gamma_R x_r^2 + \gamma_P = 0,$$

which are of course the previous values $\tilde{x}_2^{\pm}$ given in (16). The jacobian matrix of the system (20)-(21) linearized around the equilibria $(x_r, \tilde{x}_2^{\pm})$ is expressed as

$$J^{\pm} = \begin{bmatrix} \omega_n \tilde{x}_2^{\pm} - 2\gamma_R x_r k & k(1 - 2b\tilde{x}_2^{\pm}) \\ x_r(2\gamma_R - \omega_n) & 2b\tilde{x}_2^{\pm} - 1 \end{bmatrix}, \tag{22}$$

which determinant is

$$\text{Det}(J^{\pm}) = \omega_n(1 - 2b\tilde{x}_2^{\pm})(kx_r - \tilde{x}_2^{\pm}), \tag{23}$$

and the trace

$$\text{Tr}(J^{\pm}) = (\omega_n + 2b)\tilde{x}_2^{\pm} - 2\gamma_R k x_r - 1. \tag{24}$$

Assuming $\mathbf{p}^- \in \Sigma_{as}$, we have that $\text{Det}(J^-) > 0$, because $\tilde{x}_2^- < 1/2b$ and $\tilde{x}_2^- < kx_r$. Thus, $\mathbf{p}^-$ is stable (node or focus) in Σ_{as} whenever $\text{Tr}(J^-) < 0$, that is, for $k > k_{\text{Hopf}}$ with

$$k_{\text{Hopf}} = \frac{(\omega_n + 2b)\tilde{x}_2^- - 1}{2\gamma_R x_r}, \tag{25}$$

where k_{Hopf} is the critical value of parameter k at the Hopf bifurcation. Regarding $\mathbf{p}^+$, we have $\text{Det}(J^+) < 0$ since $\tilde{x}_2^+ > 1/2b$. Therefore, it is a pseudo-saddle in the region Σ_{as}. Clearly, the pseudo-equilibrium point $\mathbf{p}^-$ must be chosen as the operating point for the feedback control system.

From the previous analysis, we can give the following result to choose the parameter k ensuring the operation of the proposed SMC design, regarding variations of parameters γ_R and γ_P.

Proposition 1: Consider system (12), where h is given in (10), with fixed parameters $x_r > 1$, $b > 0$ and $\omega_n > 0$.

(i) The parameters γ_R and γ_P must be selected such that

$$0 < \gamma_R < \frac{1}{4bx_r^2} \tag{26}$$

$$0 < \gamma_P < \frac{1 - 4\gamma_R b x_r^2}{4b}, \tag{27}$$

to guarantee the existence of the pseudo-equilibrium $\mathbf{p}^-$ (desired operating point).

(ii) The parameter k must be selected such that

$$k \in \mathbf{K} = \left\{ k > \frac{\tilde{x}_2^-}{x_r} \right\} \cap \{k > k_{\text{Hopf}}\} \tag{28}$$

to guarantee the stability of the pseudo-equilibrium $\mathbf{p}^-$, where $\tilde{x}_2^-$ is given by (16) and k_{Hopf} in (25).

Furthermore, k must be chosen sufficiently far away of k_{Hopf}, making as big as possible the unstable limit cycle around the pseudo-equilibrium $\mathbf{p}^-$. In order to design the SMC, maximum values for parameters γ_R and γ_P are previously defined and parameter k is chosen to keep the system stable.

The conditions of existence and stability for the pseudo-equilibrium $\mathbf{p}^-$, presented in Proposition 1, are illustrated in Figure 8 according to the physical parameters P, R and K of the boost converter with SMC-Washout and considering the values in Table I for the other parameters. In this case, we must choose (P, R, K) within the solid shown in (a). Sections of this solid are shown in (b), (c) and (d), where the stability region is indicated by grey color areas.

IV. SIMULATION RESULTS

In this section, simulation results obtained with PSIM software in order to validate the proposed controller performance under load variations are shown. The circuit parameters are given in Table I and the simulation diagram compose of two cascaded interconnected power converters is shown in Fig. 9.

Table I
CIRCUIT PARAMETERS PC1

Input voltage	V_{in}	$12\,V$
Output voltage	v_r	$24\,V$
Inductance	L	$2.2\,mH$
Output capacitance	C	$47\,\mu F$
Inductor series resistance	r_L	$0.07\,\Omega$
Natural frequency	ω	$3110\,rad/s$
Resistive load	R	$115\,\Omega$

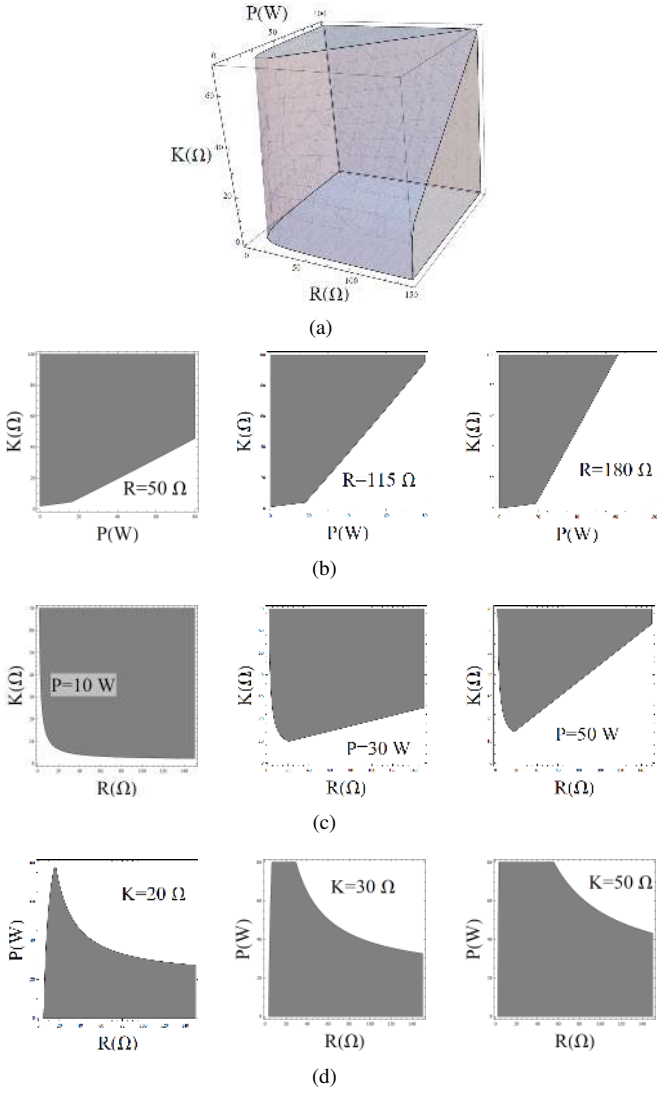

Figure 8. a) Stability region in the parameter space (P, R, K). b) (P, K)-plane for $R = 50\,\Omega, 115\,\Omega, 180\,\Omega$; c) (R, K)-plane for $P = 10\,W, 30\,W, 50\,W$; d) (R, P)-plane for $K = 20\,\Omega, 30\,\Omega, 50\,\Omega$. Stability regions are denoted by grey color areas.

Table II
CIRCUIT PARAMETERS PC2

Input voltage	v_C	$24\,V$
Output voltage	V_{ref}	$48\,V$
Maximum current	i_{max}	$2.9\,A$
Inductance	L_2	$0.5\,mH$
Output capacitance	C_2	$1\,\mu F$
Resistive load	R_2	$75\,\Omega\ -\ 230\,\Omega$

The $PC1$ boost converter is controlled by the proposed SMC. To minimize high switching frequencies that might occur in SMC, the switching function is replaced by a classical hysteresis band to limit the maximum switching frequency. The second boost converter $PC2$ that acts as a constant power load for the first converter $PC1$ and that is driving a resistive load is composed by two cascade loops: (i) an inner current control loop; and (ii) a outer voltage control loop. Both loops

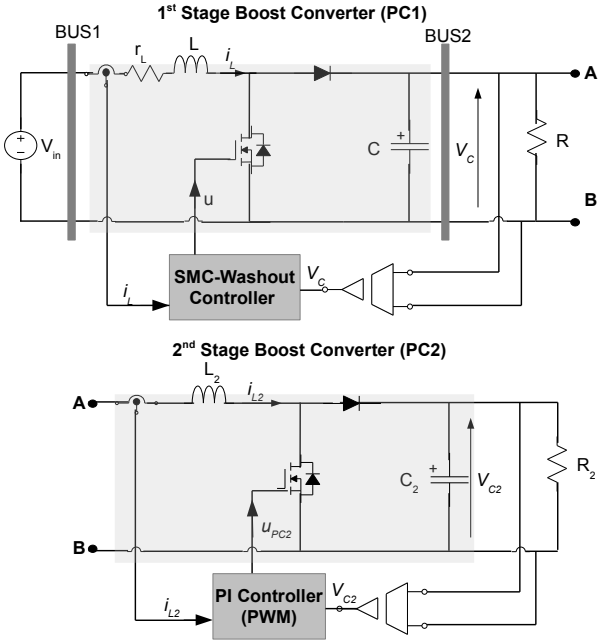

Figure 9. Two cascaded interconnected power converters showing the proposed SMC-control for the $PC1$ boost converter and a PWM nonlinear PI-control for the $PC2$ boost converter acting as a load.

have nonlinear control law, with a static nonlinearity for the inner control loop and nonlinear PI for the outer control loop. This control strategy uses a PWM to command the switch and is given by

$$u^{PC2} = \frac{1}{x_1^{PC2}}\left[1 + k_p(x_2^{PC2} - x_{2_{ref}}^{PC2})\right]$$

with

$$x_{2_{ref}}^{PC2} = x_1^{PC2}\left[k_1(x_{1_{ref}}^{PC2} - x_1^{PC2}) - k_2\int(x_1^{PC2} - x_{1_{ref}}^{PC2})dt\right]$$

where $x_1^{PC2} > 0$, x_2^{PC2} and $x_{1_{ref}}^{PC2}$ are the output voltage, inductance current and reference voltage (V_{ref}) normalized, respectively. This normalization is the same used for the PC1 converter in Section II. Normalized control parameters used to obtain the simulation results were $k_p = 0.843$, $k_1 = 0.397$, $k_2 = 0.079$ and a switching frequency of 50 KHz.

The normalized parameter values of converter $PC1$ are obtained by applying the normalization of Section II to the values given in Table I: $x_r = 2$, $x_2^* = 1.65$, $\omega_n = 1$, $b = 0.01$, $\gamma_R = 0.06$. From the resistive load variation of R_2 given in Table II, the constant power load P is calculated, i.e. $P \in [10\,W, 30\,W]$. So that applying the normalization, γ_P assumes values in the interval $[0.5, 1.5]$. According with Proposition (1), these values for the normalized parameters γ_R and γ_P guarantee the existence of the pseudo-equilibrium point $\mathbf{p}^-$ that is the desired operating point. Notice that $\tilde{x}_2^- = \tilde{x}_2^-(\gamma_P)$ is an increasing function respect to parameter γ_P, since

$$\frac{d\tilde{x}_2^-}{d\gamma_P} = \frac{1}{\sqrt{1 - 4b(\gamma_P + \gamma_R x_r^2)}} > 0,$$

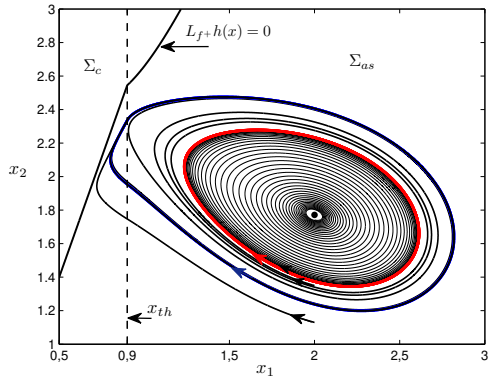

(a)

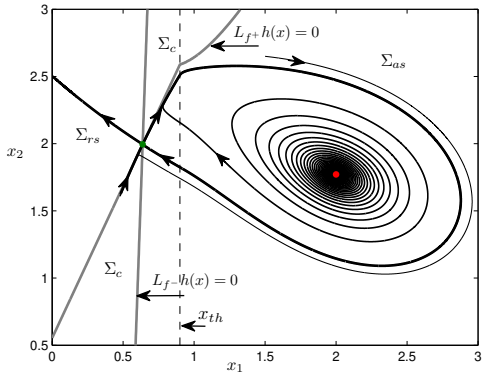

(b)

Figure 10. State-space diagram of system (12) simulated for parameters $x_r = 2$, $x_2^* = 1.65$, $\omega_n = 1$, $b = 0.01$, $\gamma_R = 0.06$ and $\gamma_P = 1.5$. a) for $k = 3.7$, showing the unstable limit cycle in red-color; the stable limit cycle in blue-color; • stands for the stable pseudo-focus. b) for $k = 3.13$, the stable limit cycle disappears when it touches a double tangency point in a HC bifurcation.

then $\tilde{x}_2^-/x_r$ and k_{Hopf} increases with γ_P. Therefore, the stabilization condition given in (28) is true adopting the maximum value for γ_P (i.e. $\gamma_P = 1.5$), thus we must take $k > 3.36$.

For the sliding dynamics, a Subcritical Hopf bifurcation occurs at $k = k_{Hopf} = 3.36$ so that there exists an unstable limit cycle around the stable pseudo-equilibrium $\mathbf{p}^-$ for $k > 3.36$; its size increases with k. Moreover, for this parameter combination there exists a stable limit cycle around this same pseudo-equilibrium point $\mathbf{p}^-$. This stable limit cycle appears rounding the unstable limit cycle and its size decreases with k (see Figure 11). Both limit cycles are confined to the attractive sliding region Σ_{as}. The stable limit cycle arises as a result of the threshold voltage x_{th}, responsible for the sliding vector field $\mathbf{f}_s$ to be piecewise smooth. The interaction of the two different dynamics ($x_1 < x_{th}$ and $x_1 \geq x_{th}$) at $x_1 = x_{th}$ gives rise to a stable limit cycle. A state space diagram in the (x_1, x_2)-plane corresponding to system (12) is shown in Figure 10(a), where it is possible to observe the unstable and stable limit cycles for $k = 3.7$. In order to determine the lower limit for the control parameter k such that the state space presents no limit cycle around $\mathbf{p}^-$, numerical continuation methods were used. The resulting bifurcation diagram is shown in Figure 11. From it we conclude that:

- The stable limit cycle exists for $k \in (3.13, 3.99)$. This limit cycle disappears for $k = 3.13$ when it touches a double tangency point ($L_{\mathbf{f}^-}h(\mathbf{x}) = L_{\mathbf{f}^+}h(\mathbf{x}) = 0$), which has a dynamics of saddle type, and also for $k = 3.99$ when it collides with the unstable limit cycle.
- The unstable limit cycle exists for $k \in (3.36, 3.99)$. This limit cycle is born in a subcritical Hopf bifurcation (H_{sub}) for $k = 3.36$ and disappears when it collides with the stable limit cycle for $k = 3.99$.
- For $k = 3.13$ a Homoclinic Connection Bifurcation (HC) occurs (see Figure 10(b)).
- For $k = 3.99$ a Saddle-Node bifurcation of periodic orbits (SNpo) occurs.

In this way, the value of the control parameter k must be chosen $k > 3.99$ in order to avoid any limit cycle around the pseudo-equilibrium point $\mathbf{p}^-$. This condition can be expressed for original system (5), from the relation $K = k\sqrt{\frac{L}{C}}$, giving $K > 27.3\,\Omega$.

Simulation results are shown in Fig. 12. In Fig. 12 (a), for $K = 24\,\Omega$, after a step in the load power P from $10\,W$ to $30\,W$ applied at time $t = 0.1\,s$ the equilibrium point becomes unstable and the voltage v_c begins to oscillate describing in the state-space a stable limit cycle. In Fig. 12 (b), for $K = 34\,\Omega$, P is changed from $10\,W$ to $30\,W$ at time $t = 0.1\,s$ and before a transient the system remains stable at the equilibrium point.

From the former analysis, control parameter K must be chosen faraway from the SN_{po} condition ($K > K_c = 27.3\,\Omega$) as indicated in Fig. 11, ensuring the stability of the proposed control design. For instance, simulation results are shown in Fig. 12 (c) for $K = 100\,\Omega$. In this picture, starting with an initial value of $P = 20$ W, at $t = 0.15$ s the power is changed to $P = 25$ W, at $t = 0.3$ s to $P = 20$ W, at $t = 0.45$ s to $P = 15$ W and at $t = 0.6$ s to $P = 20$ W.

V. CONCLUSION

This paper addressed the nonlinear analysis of interconnected power converters in DC microgrids through a case study: a cascade of two boost converters connected to a common bus. The nonlinear effects of a constant power load were analyzed and a sliding mode controller was proposed to guarantee stability under unknown load variations. The control strategy proposed was validated through simulation results. It showed a fast performance to reject load power changes. The nonlinear stability analysis performed is very useful to determine the safe parameter region for the stability system operation under power changes (parameter γ_P). This information can be summarized in bifurcation diagrams leading to practical rules for choosing the control parameter K in order to achieve a suitable SMC design.

APPENDIX
DISCONTINUOUS CONTROL SYSTEMS: CONCEPTS AND NOTATION

In this Appendix, we introduce the notation followed through the paper along with some elementary concepts about

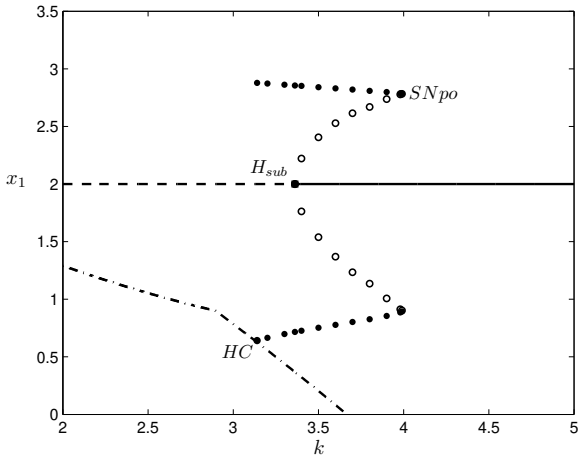

Figure 11. Bifurcation diagram in the plane (k, x_1) for k defined as the bifurcation parameter, where: — denotes a stable pseudo-equilibrium; – – an unstable pseudo-equilibrium; -.- double tangency point; • stable limit cycle; ∘ unstable limit cycle; SNpo indicates the Saddle-Node bifurcation of periodic orbits; H_{sub} stands for the Hopf bifurcation subcritical; HC indicates the homoclinic bifurcation. Parameter values are $x_r = 2$, $x_2^* = 1.65$, $\omega_n = 1$, $b = 0.01$, $\gamma_R = 0.06$ and $\gamma_P = 1.5$.

discontinuous control systems, also called Sliding Mode Control Systems (SMC), see [12] for more details. We start by considering affine control systems of the form

$$\dot{\mathbf{x}} = \mathbf{f}(\mathbf{x}) + \mathbf{g}(\mathbf{x})u \tag{A.29}$$

where $\mathbf{x} \in \mathbb{R}^n$ and the functions $\mathbf{f}(\mathbf{x})$ and $\mathbf{g}(\mathbf{x}) \neq 0$, are smooth and the control signal u is supposed to be a scalar discontinuous function. Assume a smooth non-constant scalar function $h : \mathbb{R}^n \to \mathbb{R}$ that defines the *discontinuity* manifold

$$\Sigma = \{\mathbf{x} \in \mathbb{R}^n : h(\mathbf{x}) = 0\},$$

is supposed to be regular, that is, $\nabla h(\mathbf{x}) \neq 0, \forall \mathbf{x} \in \mathbb{R}^n$, and splitting the state space into two open regions $S^- = \{\mathbf{x} \in \mathbb{R}^n : h(\mathbf{x}) < 0\}$ and $S^+ = \{\mathbf{x} \in \mathbb{R}^n : h(\mathbf{x}) > 0\}$. Accordingly, the switching control law is u, namely as

$$u = u(\mathbf{x}) = \begin{cases} u^-(\mathbf{x}), \text{ if } h(\mathbf{x}) < 0, \text{ i.e. } \mathbf{x} \in S^-, \\ u^+(\mathbf{x}), \text{ if } h(\mathbf{x}) > 0, \text{ i.e. } \mathbf{x} \in S^+, \end{cases} \tag{A.30}$$

where $u^{(\pm)}$ are scalar smooth functions of $\mathbf{x}$ (typically constant ones) to be later specified. System (A.29) endowed with the control law (A.30) constitutes a non-smooth differential system that, depending on the state, uses one of the two different smooth vector fields

$$\mathbf{f}^{(\pm)}(\mathbf{x}) = \mathbf{f}(\mathbf{x}) + \mathbf{g}(\mathbf{x})u^{(\pm)}(\mathbf{x}). \tag{A.31}$$

As usual, we look for a stable operating point $\hat{\mathbf{x}}$, belonging to the discontinuity manifold Σ, which is assumed to be a set of zero measure in $\mathbb{R}^n$. We define the rate variations of the value of h along the different orbits when extended continuously to the boundary of the open regions $S^{(\pm)}$, that is, for all $\mathbf{x} \in \overline{S^-} = S^- \cup \Sigma$ the orbital derivative of h or Lie derivative

$$L_{\mathbf{f}^-}h(\mathbf{x}) = \frac{d}{dt}h(\mathbf{x}^-(t)) = \left\langle \nabla h(\mathbf{x}), \mathbf{f}^-(\mathbf{x}) \right\rangle,$$

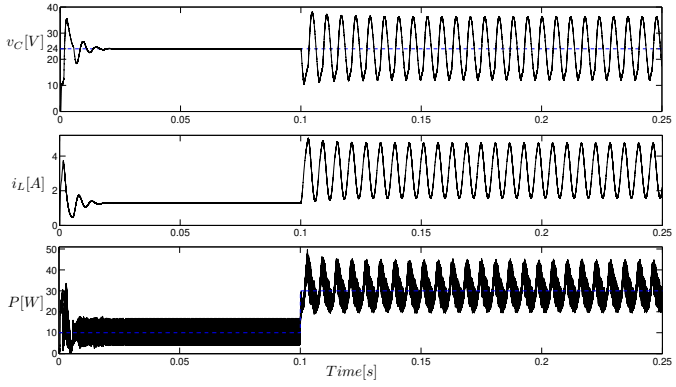

(a) $K = 24\ \Omega$

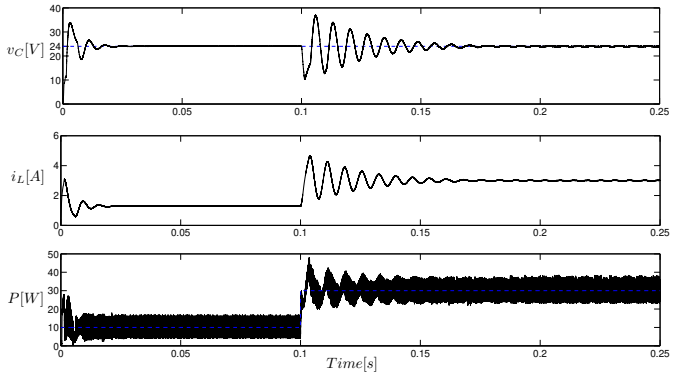

(b) $K = 34\ \Omega$

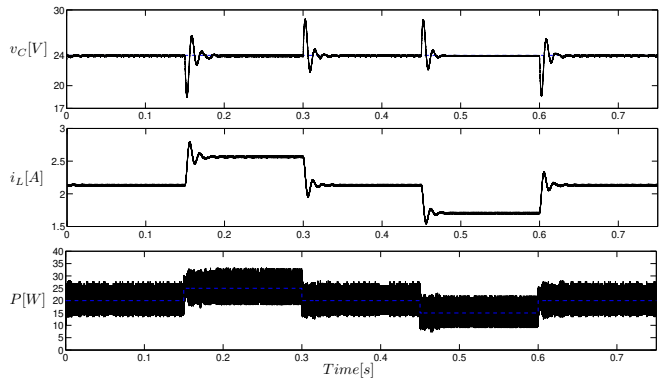

(c) $K = 100\ \Omega$

Figure 12. Time-domain responses of $i_L(t)$ and $v_C(t)$ for different steps of load power P and for three different values of the control parameter K.

and the corresponding one for all $\mathbf{x} \in \overline{S^+} = S^+ \cup \Sigma$. Note that $\Sigma = \overline{S^-} \cap \overline{S^+}$.

Then it is natural to define the *crossing* part of Σ as the Σ-open set

$$\Sigma_c = \{\mathbf{x} \in \Sigma : L_{\mathbf{f}^-}h(\mathbf{x}) \cdot L_{\mathbf{f}^+}h(\mathbf{x}) > 0\},$$

and its complement in Σ, that is the Σ-closed set

$$\Sigma_s = \{\mathbf{x} \in \Sigma : L_{\mathbf{f}^-}h(\mathbf{x}) \cdot L_{\mathbf{f}^+}h(\mathbf{x}) \leq 0\}, \tag{A.32}$$

which is normally called the *sliding* part Σ_s. Of course, we are mainly interested in its attractive part, namely the Σ-open set

$$\Sigma_{as} = \{\mathbf{x} \in \Sigma : L_{\mathbf{f}^+}h(\mathbf{x}) < 0 < L_{\mathbf{f}^-}h(\mathbf{x})\}, \tag{A.33}$$

where the two vector fields from both sides out of Σ push orbits towards Σ. From (A.31) we can also write Σ_{as} as

$$\left\{\mathbf{x}\in\Sigma : -L_{\mathbf{g}}h(\mathbf{x})u^- < L_{\mathbf{f}}h(\mathbf{x}) < -L_{\mathbf{g}}h(\mathbf{x})u^+\right\}. \quad \text{(A.34)}$$

A first goal is to define the controller for the desired operating point $\hat{\mathbf{x}}$ to belong to Σ_{as}. The two conditions in (A.33) are not sufficient for stability purposes however, since there appears in Σ_s a *sliding dynamics* induced by the interaction of the two vector fields. For robustness purposes, as stressed in the introduction, we must know as deeper as possible this sliding dynamics around the point $\hat{\mathbf{x}}\in\Sigma_s$ and its possible bifurcations.

According to Filippov's method [14], which is the most natural way of obtaining the sliding dynamics induced by the discontinuous vector field (A.29)-(A.30), we must consider the vector field

$$\mathbf{f}_s(\mathbf{x}) = \lambda\mathbf{f}^-(\mathbf{x}) + (1-\lambda)\mathbf{f}^+(\mathbf{x}), \quad \text{(A.35)}$$

where for each $\mathbf{x}\in\Sigma_s$ the value of λ should be selected such that $L_{\mathbf{f}_s}h(\mathbf{x}) = \langle\nabla h(\mathbf{x}), \mathbf{f}_s(\mathbf{x})\rangle = 0$. Imposing such condition, the *sliding vector field* becomes

$$\mathbf{f}_s(\mathbf{x}) = \frac{L_{\mathbf{f}^+}h(\mathbf{x})\mathbf{f}^-(\mathbf{x}) - L_{\mathbf{f}^-}h(\mathbf{x})\mathbf{f}^+(\mathbf{x})}{L_{\mathbf{f}^+}h(\mathbf{x}) - L_{\mathbf{f}^-}h(\mathbf{x})}, \quad \text{(A.36)}$$

which clearly simplifies to

$$\mathbf{f}_s(\mathbf{x}) = \mathbf{f}(\mathbf{x}) - \frac{L_{\mathbf{f}}h(\mathbf{x})}{L_{\mathbf{g}}h(\mathbf{x})}\mathbf{g}(\mathbf{x}). \quad \text{(A.37)}$$

It is also usual to introduce the notation

$$\mathbf{f}_s(\mathbf{x}) = \mathbf{f}(\mathbf{x}) + \mathbf{g}(\mathbf{x})u_{eq} \quad \text{(A.38)}$$

where

$$u_{eq} = -\frac{L_{\mathbf{f}}h(\mathbf{x})}{L_{\mathbf{g}}h(\mathbf{x})} = -\frac{\langle\nabla h(\mathbf{x}), \mathbf{f}(\mathbf{x})\rangle}{\langle\nabla h(\mathbf{x}), \mathbf{g}(\mathbf{x})\rangle} \quad \text{(A.39)}$$

is the so called *equivalent control*, see [15]. We note that the transversality condition $L_{\mathbf{g}}h(\mathbf{x})\neq 0$ is a necessary condition for the existence of u_{eq}.

We recall that the discontinuous system (A.29) inherits the equilibria of each vector field $\mathbf{f}^{\pm}(\mathbf{x})$, and that they can be real or virtual equilibria. In particular, we call (i) *admissible or real equilibrium points* to both the solutions of $\mathbf{f}^-(\mathbf{x}) = 0$ that belong to S^- and the solutions of $\mathbf{f}^+(\mathbf{x}) = 0$ that belong to S^+; (ii) *non admissible or virtual equilibrium points* are both the solutions of $\mathbf{f}^-(\mathbf{x}) = 0$ that belong to S^+, and the solutions of $\mathbf{f}^+(\mathbf{x}) = 0$ that belong to S^-. Virtual equilibria are not true equilibrium points, but they can play a role in the dynamics for the corresponding region.

Regarding now the dynamical system corresponding to the vector field $\mathbf{f}_s(\mathbf{x})$ induced on the sliding set Σ_s, and following [16] we call *pseudo-equilibrium points* to the solutions of $\mathbf{f}_s(\mathbf{x}) = 0$, with $\mathbf{x}\in\Sigma_s$. Pseudo-equilibrium points are, in some sense, almost true equilibria for system (A.29). For instance, suppose both vectors $\mathbf{f}^{(\pm)}$ are transversal to Σ and anti-collinear at a certain point of this surface, that is, there exist $\lambda_1,\lambda_2>0$, such that $\lambda_1\mathbf{f}^-(\mathbf{x})+\lambda_2\mathbf{f}^+(\mathbf{x}) = 0$. The point is necessarily in Σ_s, since then $L_{\mathbf{f}^{(\pm)}}h(\mathbf{x})$ are non-zero and with different sign. In fact, it is immediate to conclude that at such point one has $\mathbf{f}_s(\mathbf{x}) = 0$, being a pseudo-equilibrium for (A.29). Reciprocally, if $\mathbf{x}$ is a point of Σ_s with $\mathbf{f}_s(\mathbf{x}) = 0$ and it is not a tangency point, both vector fields are anti-collinear at the point. If for instance at such point we assume $L_{\mathbf{f}^+}h(\mathbf{x}) < 0 < L_{\mathbf{f}^-}h(\mathbf{x})$, i.e. $\mathbf{x}\in\Sigma_{as}$, we conclude that two orbits, one in S^- and another in S^+, collide with opposite directions and determine a rest point for the global vector field. This rest point, in a different way from that of true equilibria, can be achieved in finite time from the points of these two orbits, which can be seen as defining a kind of stable one-dimensional invariant manifold for the pseudo-equilibrium point.

Proposition 2: Under the assumption $L_{\mathbf{g}}h(\mathbf{x}) < 0$ for all $\mathbf{x}\in\Sigma_{as}$, the *de-singularized sliding vector field*

$$\mathbf{f}_{ds}(\mathbf{x}) = L_{\mathbf{f}}h(\mathbf{x})\mathbf{g}(\mathbf{x}) - L_{\mathbf{g}}h(\mathbf{x})\mathbf{f}(\mathbf{x}), \quad \text{(A.40)}$$

and the sliding vector field (A.37) are topologically equivalent in Σ_{as}, that is they have identical orbits and the systems are distinguished only by the time parametrization along the orbits. Therefore, pseudo-equilibria of (A.37) are also equilibria for (A.40) and the discontinuity manifold Σ remains invariant under the flow generated by $\mathbf{f}_{ds}$.

Proof. See [17].

If $L_{\mathbf{g}}h(\mathbf{x}) = 0$ for some $\mathbf{x}\in\Sigma_s$, then we have $L_{\mathbf{f}^-}h(\mathbf{x}) = L_{\mathbf{f}^+}h(\mathbf{x}) = 0$, and from (A.32) this common value vanishes. Thus the point belongs to the boundary of Σ_{as}, where the two tangency sub-manifolds of Σ intersect, and is called a *singular sliding point* (double tangency point). Furthermore, if $\mathbf{x}$ is a singular sliding point of the vector field (A.37) then it is a standard equilibrium point for the de-singularized sliding vector field, so that $\mathbf{f}_{ds}(\mathbf{x}) = 0$. See [18] for details about possible intricate dynamics around these points.

Also, we can take advantage of the invariance of Σ under the flow determined by $\mathbf{f}_{ds}$ and, after a change of variables if necessary, reduce the dimension of the problem by one. This can be done in most cases by a simple projection of the dynamics in Σ onto one of the coordinate planes; it suffices to eliminate one of the state variables through the condition $h(\mathbf{x}) = 0$ defining Σ.

The moral of the above approach is that, once assured the attractive character of Σ_{as}, although we cannot forget the global dynamics, we can focus our attention on the $\mathbf{f}_{ds}$-dynamics on Σ, and specially on Σ_{as}. The usefulness of this methodology becomes clarified in Section III.

ACKNOWLEDGMENT

This work was partially supported by the Coordenadoria de Aperfeicoamento de Pessoal de nível Superior (CAPES), Brazil. The authors also thank Vinicius Stramosk and Eduardo Lenz for your help in the analysis of the system studied in this paper. L. Benadero was supported by the Spanish *Ministerio de Ciencia e Innovación* under grant DPI2013-47293-R and E. Ponce by MINECO/FEDER grant MTM2012-31821 and by the *Consejería de Economía, Innovación, Ciencia y Empleo de la Junta de Andalucía* under grant P12-FQM-1658.

REFERENCES

[1] D. Boroyevich, I. Cvetkovic, D. Dong, R. Burgos, F. Wang, and F. Lee, "Future electronic power distribution systems a contemplative view," in *12th International Conference on Optimization of Electrical and Electronic Equipment (OPTIM)*, 2010, pp. 1369–1380.

[2] D. Boroyevich, I. Cvetkovic, R. Burgos, and D. Dong, "Intergrid: A future electronic energy network?" *IEEE Journal of Emerging and Selected Topics in Power Electronics*, vol. 1, no. 3, pp. 127–138, Sept. 2013.

[3] R. Haroun, A. Cid-Pastor, A. El Aroudi, and L. Martinez-Salamero, "Synthesis of canonical elements for power processing in dc distribution systems using cascaded converters and sliding-mode control," *IEEE Trans. on Power Electronics*, vol. 29, no. 3, pp. 1366–1381, March 2014.

[4] R. Haroun, A. El Aroudi, A. Cid-Pastor, G. Garica, C. Olalla, and L. Martinez-Salamero, "Impedance matching in photovoltaic systems using cascaded boost converters and sliding-mode control," *IEEE Trans. on Power Electronics*, vol. 30, no. 6, pp. 3185–3199, June 2015.

[5] X. Xiong, C. K. Tse, and X. Ruan, "Bifurcation analysis of standalone photovoltaic-battery hybrid power system," *IEEE Trans. on Circuits and Systems-I: regular papers*, vol. 60, pp. 1354–1365, 2013.

[6] ——, "Smooth and nonsmoooth bifurcations in multi-structure multi- operating-mode hybrid power systems," *Int. J. Bifurcation and Chaos*, vol. 23, 2013.

[7] E. Lenz and D. J. Pagano, "Nonlinear control for bidirectional power converter in a dc microgrid," in *9th IFAC Symposium on Nonlinear Control Systems, Toulouse, France*, Sept. 2013, pp. 359–364.

[8] A. P. N. Tahim, D. J. Pagano, E. Lenz, and V. Stramosk, "Modeling and stability analysis of islanded dc microgrids under droop control," *IEEE Trans. on Power Electronics*, vol. 30, no. 8, pp. 4597–4607, August 2015.

[9] C. N. Onwuchekwa and A. Kawasinski, "Analysis of boundary control for buck converters with instantaneous constant-power loads," *IEEE Trans. on Power Electronics*, vol. 25, no. 8, pp. 2018–2032, August 2010.

[10] A. Emadi, A. Khaligh, C. H. Rivetta, and G. A. Williamson, "Constant power loads and negative impedance instability in automotive systems: definition, modeling, stability, and control of power electronic converters and motor drives," *IEEE Trans. on Vehicular Technology,*, vol. 55, no. 4, pp. 1112–1125, 2006.

[11] V. Stramosk, L. Benadero, D. J. Pagano, and E. Ponce, "Sliding mode control of interconnected power electronic converters in dc microgrids," in 39^{th} *Annual Conference of the IEEE Industrial Electronics Society, IECON 2013*, November 2013, pp. 8385–8390.

[12] E. Ponce and D. J. Pagano, "Sliding dynamics bifurcations in the control of boost converters," in *Preprints of the 18th IFAC World Congress, Milano, Italy*, 2011, pp. 13 293–13 298.

[13] A. P. N. Tahim, D. J. Pagano, and E. Ponce, "Nonlinear control of dc-dc bidirectional converters in stand-alone dc microgrids," in *51st Annual Conference on Decision and Control (CDC)*, December 2012, pp. 3068–3073.

[14] A. F. Filippov, *Differential Equations with Discontinuous Right-hand Sides*. Kluwer Academic Publishers, Dordrecht, The Netherlands., 1988.

[15] V. I. Utkin, *Sliding Modes in Control Optimization*. Springer, 1992.

[16] Y. A. Kuznetsov, S. Rinaldi, and A. Gragnani, "One parameter bifurcations in planar Filippov systems," *Int. J. Bifurcation and Chaos*, vol. 8, no. 13, pp. 2157–2188, 2003.

[17] D. J. Pagano and E. Ponce, "Sliding mode controllers design through bifurcation analysis," in *Preprints of the 8th IFAC on Nonlinear Control Systems, Bologna, Italy*, 2010, pp. 1284–1289.

[18] M. R. Jeffrey and A. Colombo, "The two-fold singularity of discontinuous vector fields," *SIAM J. Appl. Dyn. Syst.*, vol. 8, no. 8, pp. 624–640, 2009.

Luis Benadero was born in Ciudad Real (Spain) in 1952, received the Ph.D. degree from the Universitat Politcnica de Catalunya (UPC) in 1983. Formerly he was with the UPC Department of Electronic Engineering and currently he is an Associate Professor with the Applied Physics Department. His research activity has been related to nonlinear phenomena. Currently he is mainly focused in nonlinear dynamics, more specifically for piecewise smooth systems. Such systems have an important application in power electronics, subject in which he has published several papers in the two last decades.

Rony Cristiano was born in Ararangua, Santa Catarina, Brazil. He received the degree in mathematics, the Ms.C. degree in automatic control systems engineering from the Federal University of Santa Catarina, Brazil, in 2010 and 2013, respectively. He is currently a Ph.D. student of the automatic and systems engineering program at the Federal University of Santa Catarina. His research interest are in the area of nonlinear dynamical systems, discontinuous dynamical systems, control systems, bifurcation analysis and power electronics.

Daniel J. Pagano was born in La Plata, Argentine, in 1961. He received the B.Sc. degree in Telecommunications Engineering from National University of La Plata, Argentine, in 1985. M.Sc. degree in Electrical Engineering from Federal University of Santa Catarina, Brazil, in 1989 and Ph.D. degree in Robotics, Automation and Electronics from the University of Seville, Spain, in 1999. He is currently a Professor at the Dept. of Automation and Systems, Federal University of Santa Catarina, Brazil. His main research interests include nonlinear dynamical systems, bifurcation analysis, nonlinear control, power electronics and microgrids.

Enrique Ponce was born in Seville, Spain, on July 2nd, 1955. He received the Ingeniero Industrial and Doctor Ingeniero Industrial degrees from the University of Seville, Seville, Spain, in 1978 and 1987, respectively. Since 1978, he has been with the Department of Applied Mathematics at the University of Seville, where he is currently a Professor. His research interests are nonlinear oscillations, bifurcations and piecewise linear systems, with emphasis on applications in nonlinear control and electronics.